Nanotechnology

PAPER • OPEN ACCESS

Time-resolved open-circuit conductive atomic force microscopy for direct electromechanical characterisation

To cite this article: Yonatan Calahorra *et al* 2020 *Nanotechnology* **31** 404003

View the article online for updates and enhancements.

IOP ebooks™

Bringing together innovative digital publishing with leading authors from the global scientific community.

Start exploring the collection–download the first chapter of every title for free.

This content was downloaded from IP address 128.178.141.186 on 17/08/2020 at 10:19

OPEN ACCESS
IOP Publishing
Nanotechnology

Nanotechnology **31** (2020) 404003 (12pp)
https://doi.org/10.1088/1361-6528/ab9b4b

Time-resolved open-circuit conductive atomic force microscopy for direct electromechanical characterisation

Yonatan Calahorra[1], Wonjong Kim[2], Jelena Vukajlovic-Plestina[2], Anna Fontcuberta i Morral[2,3] and Sohini Kar-Narayan[1]

[1] Department of Materials Science and Metallurgy, University of Cambridge, CB3 0FS, Cambrdige, United Kingdom
[2] Laboratory of Semiconductor Materials, Institute of Materials, School of Engineering, Ecole polytechnique fédérale de Lausanne (EPFL), 1015 Lausanne, Switzerland
[3] Institute of Physics, School of Basic Sciences, Ecole polytechnique fédérale de Lausanne (EPFL), 1015 Lausanne, Switzerland

E-mail: yc402@cam.ac.uk and sk568@cam.ac.uk

Received 9 April 2020, revised 26 May 2020
Accepted for publication 10 June 2020
Published 16 July 2020

Abstract

Studying nanomaterial piezoelectricity and triboelectricity is attractive for energy and sensing applications. However, quantitative characterisation of electromechanical effects in nanomaterials is challenging due to practical limitations and possible combination of effects, resulting in contradicting reports at times. When it comes to piezoelectricity at the nanoscale, piezoresponse force microscopy (PFM) is the default characterisation tool. In PFM the converse piezoelectric effect is measured - the conversion from electrical signal to mechanical response. However, there is an underlying desire to measure the direct piezoelectric effect - conversion of mechanical deformation to an electrical signal. This corresponds to energy harvesting and sensing. Here we present time-resolved open-circuit conductive atomic force microscopy (cAFM) as a new methodology to carry out direct electromechanical characterisation. We show, both theoretically and experimentally, that the standard short-circuit cAFM mode is inadequate for piezoelectric characterisation, and that resulting measurements are governed by competing mechanisms. We apply the new methodology to nanowires of GaAs, an important semiconductor, with relatively low piezoelectric coefficients. The results suggest that time-resolved operation distinguishes between triboelectric and piezoelectric signals, and that by measuring the open-circuit voltage rather than short-circuit current, the new methodology allows quantitative characterisation of the vertical piezoelectric coefficient. The result for GaAs nanowires, ~ 1–3 pm V^{-1}, is in good agreement with existing knowledge and theory. This method represents a significant advance in understanding the coexistence of different electromechanical effects, and in quantitative piezoelectric nanoscale characterisation. The easy implementation will enable better understanding of electromechanics at the nanoscale.

Supplementary material for this article is available online

Keywords: AFM, piezoelectricity, triboelectricity, nanowires, energy harvesting

(Some figures may appear in colour only in the online journal)

Original Content from this work may be used under the terms of the Creative Commons Attribution 4.0 licence. Any further distribution of this work must maintain attribution to the author(s) and the title of the work, journal citation and DOI.

1. Introduction

1.1. Background

The search for sustainable and ubiquitous energy sources [1], combined with the several decades long interest in semiconductor nanowires [2] (NWs) has brought focus to a topical niche - that of piezoelectric semiconductor NWs. This field, largely pioneered by Wang *et al* [3–5], offers potential applications in sensing, energy harvesting and logic [6–8]. Three distinct electromechanical effects are manifested in piezoelectric semiconductor nanowires: i) the high aspect ratio allows large elastic deformations, therefore enhancing the piezoelectric effect [3], describing changes in surface polarisation due to applied strain; ii) increased surface-to-volume ratio enhances interfacial effects such as triboelectricity [9, 10], relating to surface charge transfer upon contact with a dissimilar material; iii) the combination of semiconducting and piezoelectric properties results in a unique electromechanical phenomenon coined the piezotronic effect [6, 11], whereby the height of a semiconductor energy barrier for charge carrier transport is changed due to mechanical pressure. See appendix A for a short review of the three mechanisms and basic equations. The work presented here aims to distinguish these effects in conductive atomic force microscopy (cAFM).

When considering electromechanical current/voltage generation from semiconductor NWs, both single NWs and NW ensembles or arrays have been considered [12–15]. In particular, an abundance of cAFM measurements have been reported on piezoelectric semiconductor NWs (mostly ZnO and III-N). In cAFM, the tip is scanned along the surface, while the current is recorded simultaneously, usually under applied bias. This mode of operation is also useful for other physical mechanism characterisation, such as photovoltaics [16]. However, straightforward application of cAFM for electromechanical characterisation of piezoelectric NWs is challenging. The two common variants for piezoelectric NW characterisation are: i) the short-circuit cAFM - recording the current generated by deforming a NW with an AFM tip [12, 15, 17, 18]; ii) the loaded configuration (resiscope mode): recording the voltage developed across a resistor in parallel to the deformed NW [4, 13, 14, 19, 20].

Although this is a widely studied topic and a commonly conducted experiment, very little attention has been given to the complete set of mechanically induced current flow mechanisms, namely piezoelectric, triboelectric and piezotronic. The combination of these effects is to be expected due to the nature of measurement involving dynamic forces and contact characteristics experienced by the NW-tip system, as the tip is scanned in and out of contact with NWs. Indeed, we are aware of only two reports attempting a quantitative analysis of the measured voltage or current [18, 19], to extract or compare the piezoelectric coefficients with theory - albeit with limited success.

The contrast between abundant experimental demonstrations of electrical generation from piezoelectric NWs and lack of quantitative discussion, is closely related to an uncertainty in the physical origins of the measured signals. In particular, the initial report on cAFM based generation from ZnO NW [4], was followed by alternative analysis of the results [21, 22], and a rebuttal from Wang [23]. Furthermore, flat ferroelectric samples have been studied by similar approaches [24–26]. In particular, a direct piezoresponse force microscopy (PFM) method, introduced by Gomez *et al* [25], was used to quantitatively extract direct piezoelectric coefficients; however, the nature of that method precludes its application to nanomaterials, or materials of lower piezoelectric coefficients, as discussed below.

Herein, we report a new methodology to perform this experiment, enabling reliable extraction of the piezoelectric coefficients using cAFM. The prevailing method for quantitative analysis of piezoelectricity is PFM, which is generally not suitable for non-planar samples [27], and characterises converse piezoelectricity (electrical to mechanical). We performed a detailed set of cAFM experiments at different conditions to isolate and distinguish the various current mechanisms in vertical pressure based cAFM measurements. Using scanning and ramp-mode cAFM in conjunction, we show that all three current mechanisms mentioned here (A) are present in the case of GaAs NWs.

We also show that the piezotronic and triboelectric currents can dominate the measurements to the point of obscuring piezoelectric data. We distinguish between short- and open-circuit configurations, and their practical applications in relation to cAFM based measurements. We suggest an open-circuit configuration and a time-resolved measurement methodology to extract the piezoelectric coefficients, demonstrating good agreement to known values of GaAs. Obtaining these numbers for GaAs, a weak piezoelectric material, indicates promise to use with other piezoelectric materials. Our method offers a route for quantitative analysis of the direct piezoelectric effect. It is easily implemented, and can be extended to other piezoelectric nanostructures, as well as to characterise triboelectricity.

1.2. Electromechanical cAFM measurements of semiconductor NWs

The commonly reported cAFM measurement of vertically aligned (as-grown) NWs is based on bending-induced current generation. This is due to two reasons, related to the geometry of the AFM tip/NW system: i) ideally, contact mode piezoresponse force microscopy (PFM [28, 29]) would have been desirable to measure the piezoelectric properties of the NW, and specifically the axial piezoelectric coefficient. However, NWs are brittle when considering contact mode operation, and therefore such reports are scarce, and require mechanical constraints [30]. We have previously addressed this issue by developing a non-destructive PFM operation mode [27] and applying it to horizontal and vertical III-V NWs [31]. This limitation, together with the need to characterise the direct piezoelectric effect (rather than the converse effect in the case of PFM), has directed work towards electromechanical cAFM; ii) while slender NWs are easily bent, their axial stiffness is considerably larger (see B); hence, the common cAFM NW

characterisation methodology measures current during bending while the tip is scanned across the NWs. The electromechanical response of a bending NW is more complicated than axial compression/extension, making analysis of these measurements harder to begin with.

The common description of NW deformation-induced current generation measurements is as follows [4, 23]: as the tip is scanned across the sample and a NW is bent, the compressed and stretched sides of the NW develop a potential difference. A current flows when the tip is in contact with one of these sides. Interestingly, the common observation is that only one of the voltage polarities is associated with measurable current flow. This is attributed to the rectifying electrical properties of the tip-NW contact [4]. Notably, this is in contrast to the common observation in NW ensemble device measurements, where two current/voltage peaks of opposite sign are associated with straining and relaxing the device [32, 33]. Moreover, the role of the rectifying contact is deemed even more fundamental. It was found that the existence of a rectifying contact is critical for electrical generation by the strain/compression of the piezoelectric semiconductor nanowire, to prevent a non-efficient current route (*i.e.* involving power dissipation within the NW) developing between the polarised regions of the NW [4, 13–15, 34]. The underlying reasoning could be that NWs with good electrical contacts are in fact highly doped, and their piezoelectric properties deteriorate. These points have been a part of the discussion regarding the origins of the measured signal, where alternative explanations were suggested, related to the instrumentation [21, 22]. Our work offers a comprehensive examination of this issue, and possible explanation to a wide range of experimental results.

2. Materials and methods

2.1. Nanowire growth and morphology

Ga-catalyzed GaAs NWs were grown on doped silicon by molecular beam epitaxy (MBE), in a process similar to previous reports [35–37]. The samples contained both wurtzite and zinc-blende NWs, however there was no certainty towards the structure of a specific NW measured. See supporting information section S1 (stacks.iop.org/NANO/31/404003/mmedia) for full details.

2.2. AFM characterisation

For AFM characterisation, the sample back side was sputtered with gold, and mounted on a circular metallic AFM holder using silver paint. Atomic force microscopy was carried out using a *Bruker* Dimension Icon microscope, using the PF-TUNA mode, through scanning, I-V and I-Z (ramping) operation. In PF-TUNA scanning mode, the tip is periodically oscillated (low frequency ~ 0.5–2 kHz) above the surface such that it forms intermittent contact with the sample, up to a specified force *i.e.* the peak-force. The steady state deflection is monitored as a feedback signal to find the specified peak-force. No current feedback was used. The tips used were MESP-RC-V2 (coated silicon) by Bruker, and Adama AD-40-AS (diamond tips, to prevent tip damage; all time-resolved measurements reported were done using these tips). To realise an open-circuit configuration a standard glass slide was introduced between the conductive AFM stage and the sample holder. The general experimental procedure was: i) locating a NW through a ~ 10-15 μm scan, zooming-in, switching to ramp mode in the desired location, where the current was recorded during ramping with controlled rate and force. The force in ramp mode was significantly larger (about 1000 nN) than the force in scanning mode (about 100 nN). The geometry of the NWs here allows this kind of top load as only at the maximal force the NW is close to its buckling limit (see B).

2.3. Analysis

Growth analysis was done using scanning electron microscopy (SEM, Zeiss MERLIN). AFM results were analysed using NanoScope Analysis software, and MATLAB was used for calculations and presentation of results.

3. Results and discussion

3.1. Pressure-dependent contact current

figure 1(a) shows a schematic of the experimental PF-TUNA procedure [38], where the AFM tip is periodically indenting the sample while rastering across the sample and recording the resulting current. Figure 1(b) shows a SEM image of the examined NW sample. Nanowire growth time was controlled to maintain a relatively short length, rendering the NWs more stable under AFM scanning. Noticeably, alongside the NWs, parasitic growth dominates the silicon surface, on which the NWs were grown by molecular beam epitaxy (MBE).

figure 2 shows a set of PF-TUNA current maps obtained from a NW (topography in black and white), with increasing peak-force (the maximum mechanical load, see Methods section) values of 20-60 nN. The electrical response area increased with the mechanical stimulus, however the highest current was measured at 45 nN peak force. This indicates that the relation between the measured current and applied force is not straightforward. Furthermore, the current was not correlated to the top of the NW, but to a region along its side, found to be consistent throughout the measurements. This result could be explained with an increased deformation of this side, however the measured current was found to be uncorrelated with the deformation maps (supporting information figure S1), and this result recurred throughout this work. Moreover, this observation was reinforced through measurements obtained from the sample in general: zero-bias current is observed throughout the sample, upon contact with the surface, and the parasitic GaAs growth (see figure S2). Bearing in mind that the parasitic growth is not expected to produce a significant piezoelectric signal, and is irregularly deformed, we conclude that the current observed is not piezoelectric per se, and we associate the pressure dependence with improved electrical contact (see below and supporting information figure S3). The following set of experiments explore the two additional electromechanical current mechanisms.

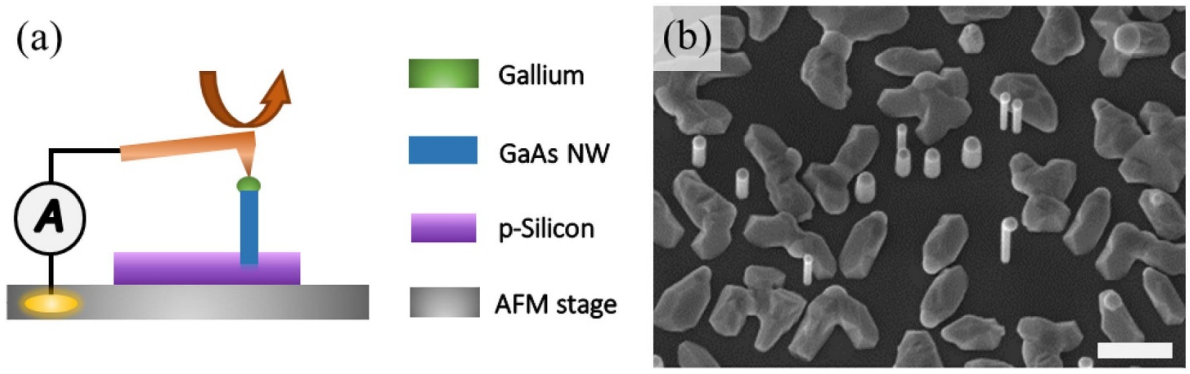

Figure 1. (a) Measurement schematic, showing the AFM cantilever descending atop the NW, and the current measured; (b) the sample used in these measurements viewed by SEM in an angle of 20°. Scale bar is 1 μm.

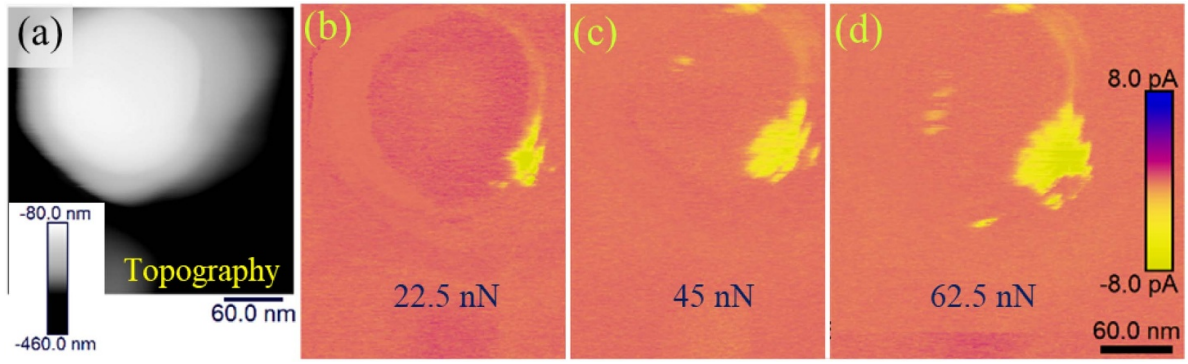

Figure 2. Scanning peak-force influence on measured short-circuit current map (a) single NW height channel; (b,c,d) contact current maps obtained with 22.5, 45, 62.5 nN peak-force. The active area increased with applied force.

3.2. Bias-dependent contact current

To further explore the nature of the measured current, a small bias was applied to the sample during scanning. Figure 3 shows current maps obtained with lower/higher peak force setting (top and bottom) and three biasing conditions: negative, zero and positive. The bias used was ± 10 mV. The central column of figure 3 is similar to figure 2, where increased peak force results in broader current 'hot-spots'. The bias sign was found to dictate the measured current sign. This is another indication that the measured hot-spot current is not piezoelectric. The increase in current hot-spot area with pressure could indicate that the dominant mechanism is improvement of the contact, and not piezoelectricity. We note that, following this experiment, we have found that there is an electrical ground imbalance in the instrument of about 3.5 mV, which probably contributes to the current measured in zero bias.

I-V measurements taken from the current hot-spots and the low-current areas on top of the NW show a complementary picture where the low-current areas show a rectified I-V curve, while the hot-spots show better conductivity. This is most likely related to the geometry of the NW and tip, and a local barrier reduction due to Schottky effect (Supporting Information figure S3). In these experiments, there were no conclusive findings relating the current to applied pressure, *i.e.* the piezotronic effect.

Furthermore, since GaAs is considered here, there might be an optoelectronic contribution to the current through carrier generation by the AFM laser, as demonstrated recently by Alekseev *et al* [18]. It is therefore of interest to eliminate steady-state (ohmic/piezotronic) contributions to the current.

3.3. Open-circuit current measurements

In order to reduce unwanted steady-state current contributions, we introduced a standard microscope glass slide between the sample and the AFM stage; this is schematically shown in figure 4(a). Notably, the existence of a 'steady-state' electrical contact (*i.e.* ohmic or rectifying contact) is not necessary for the observation of generated current/voltage in piezoelectric generators [32, 33]. This is obvious when considering the issue outside the context of piezoelectric semiconductors: the best piezoelectric materials are insulating, and therefore do not have good electrical contacts. If so, the central role of the Schottky contacts in cAFM measurements of electromechanically induced current (as mentioned above) implies that this current is indeed not purely due to piezoelectricity. Therefore, we set out to examine cAFM-induced current in an open-circuit configuration.

Figures 4(b) and (c) provides complementary results to figure 3, obtained under open-circuit conditions. The current was

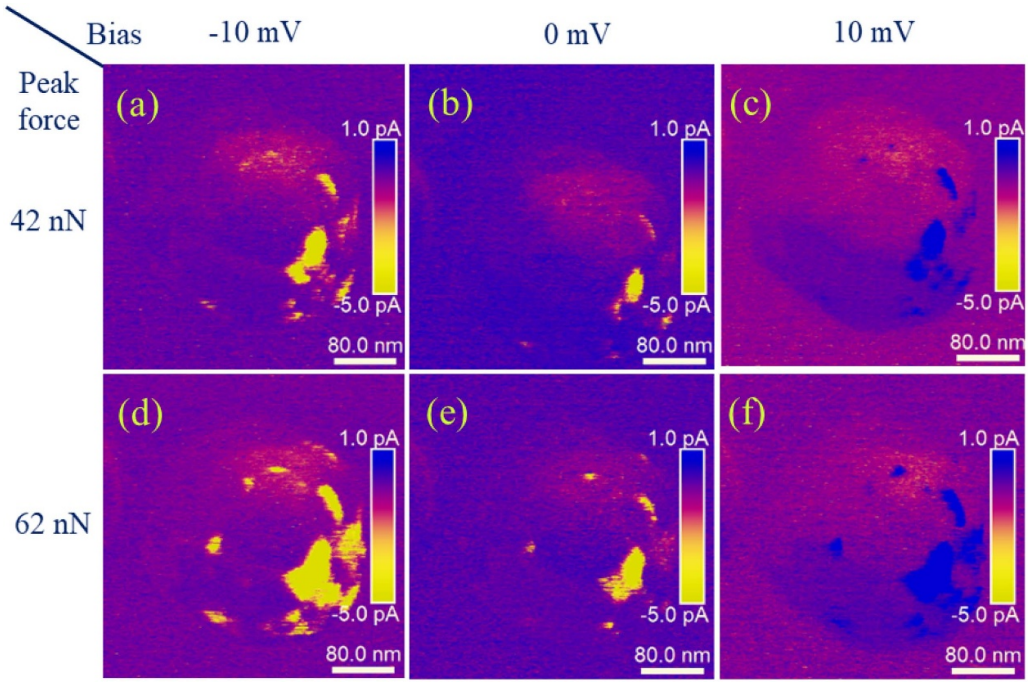

Figure 3. Bias influence on measured current map. Contact current maps obtained with 42 or (d-f) 62 nN peak-force, and sample-tip bias of -10/0/10 mV (a,d/b,e/c,f). The bias had a significant effect on measured current.

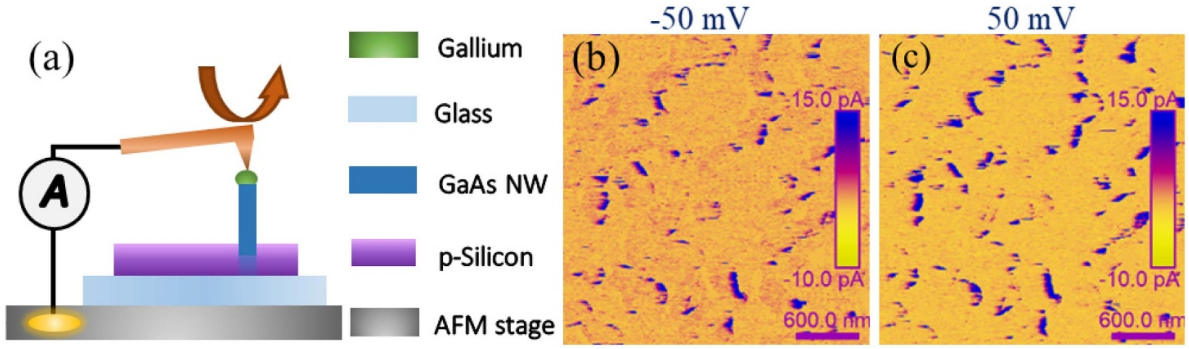

Figure 4. a) Open-circuit cAFM measurement schematic; b,c) consecutive current maps obtained from the sample while applying -50 [b], and 50 mV [c]. These images encompass both parasitic growth and nanowires which contribute to the signal. The isolation rendered the measurement not sensitive to the bias.

found to be independent of applied bias, in a striking contrast to the standard configuration. This implies that steady state currents were dominating the measurements before. Nonetheless, the measured current was still not negligible, and maintained the hot-spot characteristics. This result is intriguing: i) if ohmic/piezotronic contributions are eliminated, then triboelectric and piezoelectric currents are possible; ii) considering the uncorrelated nature of the deformation maps and the current maps, the reasonable conclusion is that triboelectricity is the dominant effect in the generation of current hot spots in the open-circuit regime. This conclusion is in good agreement with recent reports of the co-existence of triboelectricity and photovoltaic current generation in a III-V material probed by cAFM [39]. Another possible contributor to such currents is the op-amp bias current [21]. The question therefore remains: is it possible to record the piezoelectric generation arising from a single NW? [21–23]

3.4. Time-resolved current measurements

In order to further investigate electromechanical current generation, we moved on to explore the time-resolved characteristics obtained through mechanical ramping in open-circuit configuration. This has several advantages compared to the scanning mode: i) the currents in scanning mode are averaged over significant periods of time (*e.g.* the entire contact time or the entire peak-force period). Therefore time-resolved measurements provide additional information; ii) ramping is less destructive than scanning and larger forces can be used, allowing stronger indentations - thus resulting in an increased

electromechanical response. Here we drove the cantilever into the sample up to a force of ~ 1300 nN, which is roughly 10 times larger than the peak-force used during scanning.

Figure 5 shows time-resolved current measurements obtained from a current hot-spot and from the top of the NW, where generally low currents were found. The top part of the image shows the scanning results, demonstrating once more the lack of correlation between deformation and current. Low- and high-current spots were chosen, and a series of mechanical ramps with a preset maximal force were executed, while changing the ramping rate from 20 nm/sec (left-hand side) to 505 nm/sec (right-hand side). The tip was completely out of touch with the sample after every measurement, as evident from the force curve plateau. The maximum applied force is represented by the difference between the peak value and the plateau value, which is lower than zero due to offset in the AFM deflection measurement.

The two ramping points gave rise to distinct traits: the current hot-spots show a current peak measured directly upon tip-sample contact, and a subsequent decay of the current. Conversely, the low-current NW top, gave rise to a current peak which is correlated with the trend of the applied force - most evident in faster (shorter) ramps. These findings support the assumption that triboelectric current is the dominant mechanism explaining the current hot-spots, considering the instantaneous onset of current and the lack of correlation with deformation (green arrows in figure 5). Possibly, the geometry of the tip and sample results in spatial locations which favour the onset of triboelectric current, for example where sharp features result in a locally enhanced electric field supporting charge transfer.

The current measured on top of the NW, with good correlation to the applied force (figure 5(e)), is an indication of piezoelectric generation. This follows the elimination of DC currents and triboelectric currents, as the dominant mechanisms in this position. However, there are still ambiguities in understanding this current: firstly, measurement of GaAs under the red AFM laser induces an inherent contribution from carrier generation, [18] and it is possible that the contact current here is affected by that mechanism. Indeed, overlaying the currents in figure 5(d) and (e) indicates that a possible background current is present during the measurement, apart from the peaks (see supporting figure S4). Secondly, the lack of an opposite current peak is intriguing: piezoelectricity is linear, and therefore it might be expected that both positive and negative currents will appear upon compressing and releasing the NW. This effect is sometimes seen in open-circuit characterisation of piezoelectric generators where the discharge route might be different than the charge route [40, 41].

3.5. Extraction of piezoelectric coefficients

For extracting the *direct* piezoelectric coefficient, it is necessary to quantify this measurement. We examine the different configurations in their electronic context in figure 6. The operation of a generator is influenced by its load, hence the piezoelectric element acts as a voltage source under open-circuit conditions, and as a current source under short-circuit conditions (figure 6(a)). Analysis of the loaded configuration is not straightforward, and indeed, the efficiency of piezoelectric energy harvesters (as of any electrical generator) is affected by the load [8, 42] (figure 6(b)).

Inversely, the open-circuit and short-circuit configurations are straightforward for (theoretical) analysis, and correspond to the piezoelectric element acting as a voltage and current source correspondingly (figure 6(c) and (d)). In particular, our implementation of the open-circuit configuration, with a capacitor in series to the device, is a voltage differentiator, where the measured current maintains the following with the capacitance (c) and voltage (v)

$$i_{measured} = c_{glass}\frac{dv}{dt} \tag{1}$$

The other components shown in figure 6 are the NW internal resistance (r_{NW}), which is expected to be high in our case, and capacitance (c_{NW}), which is determined by the surface area of a single NW and therefore very low (~ 10^{-18} F). R_A is the current to voltage converter feedback resistor, and c_p is the feedback/stray capacitance. According to AFM manufacturer $R_A \simeq 5$ GΩ and c_p~ fF - accounting for about 10 kHz operation bandwidth (private communication with *Bruker*). The glass capacitor used here is comprised of an AFM sample holder plate (1.25 cm in diameter), and the AFM stage, with a 1 mm glass slide in between. This result is $c_{glass} = 5.3$ pF, assuming relative permittivity of 5 [43]. Therefore c_{glass} is significantly larger than the other capacitors in the circuit, and comes into play. Furthermore, the time-resolved experiment does not involve rapid changes to the equivalent circuits, since the tip is in consistent contact with the NW, therefore there are no significant changes expected in the contribution of the op-amp current bias to the signal [21]; if these are present, we aim to eliminate them as constants in time.

3.5.1. Short-circuit configuration.

Short-circuit across the NW length (the piezoelectric 3-axis) indicates that (for simplicity, considering axial fields and displacements alone)

$$E_3 = 0 \tag{2}$$

$$D_3 = P_3 = d_{33}T_3 \tag{3}$$

where E is the electric field, D the electric displacement field, P the polarisation, T the stress and $d_{i,j}$ the piezoelectric charge coefficient. Since there are no fields outside the nanowire, the boundary conditions for the displacement field hold $D = \pm Q/A$, where A is the effective electrode area, and Q the free interfacial charge, neutralising the polarisation charge, brought by the deformation. Ideally, the current measured in the experiment is the movement of charges to neutralise the polarisation - a generated current (figure 6(d)).

The dimensions of the NW measured in figure 5 are $L_{NW} = 210$ nm and $r_{NW} = 70$ nm. We have tried to take the significant uncertainty in the diameter of the NW (lateral AFM

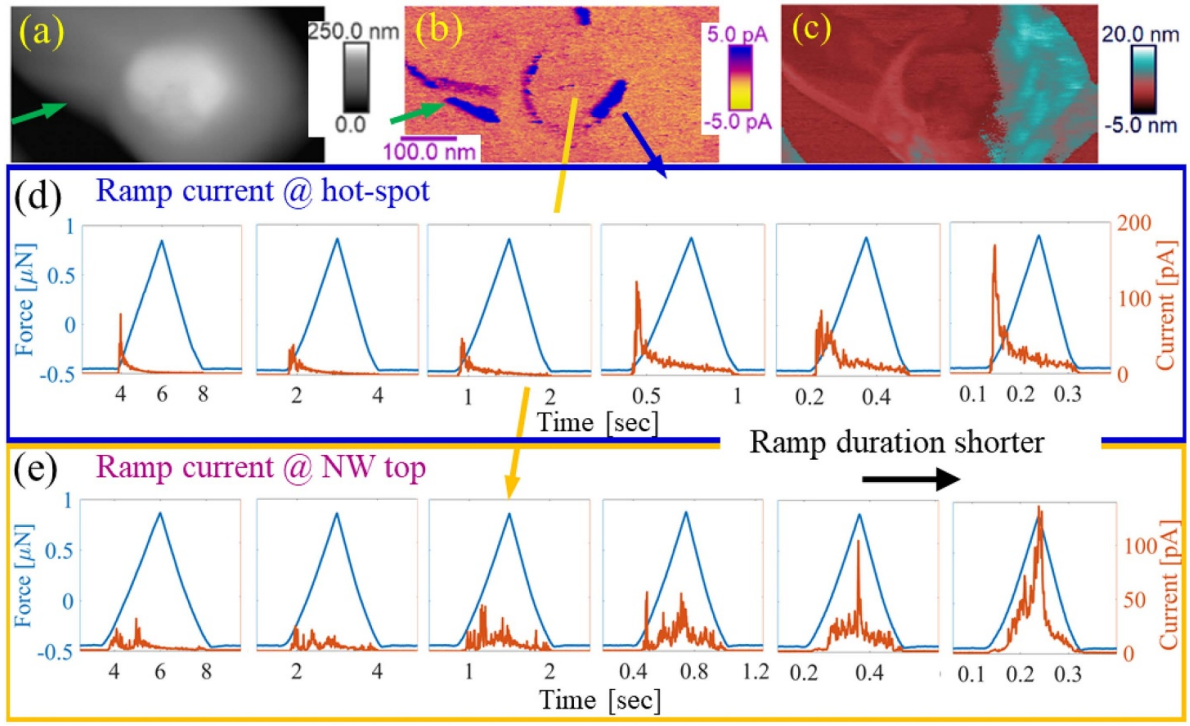

Figure 5. Mechanical ramping induced open-circuit measured current: time-resolved. (a) Topography (b) current map and (c) deformation map of a NW later used to obtain feedback-controlled time-resolved current from the high (d) and low (e) current locations; (d,e) a series of time-resolved current measurements obtained by mechanical ramping on-top the same position, to the same maximal force, with varying ramping rate. Note the current axis for (e) and (d) are not identical. low- and high-current positions yield distinct time-resolved current characteristics, interpreted as piezoelectric and triboelectric contributions.

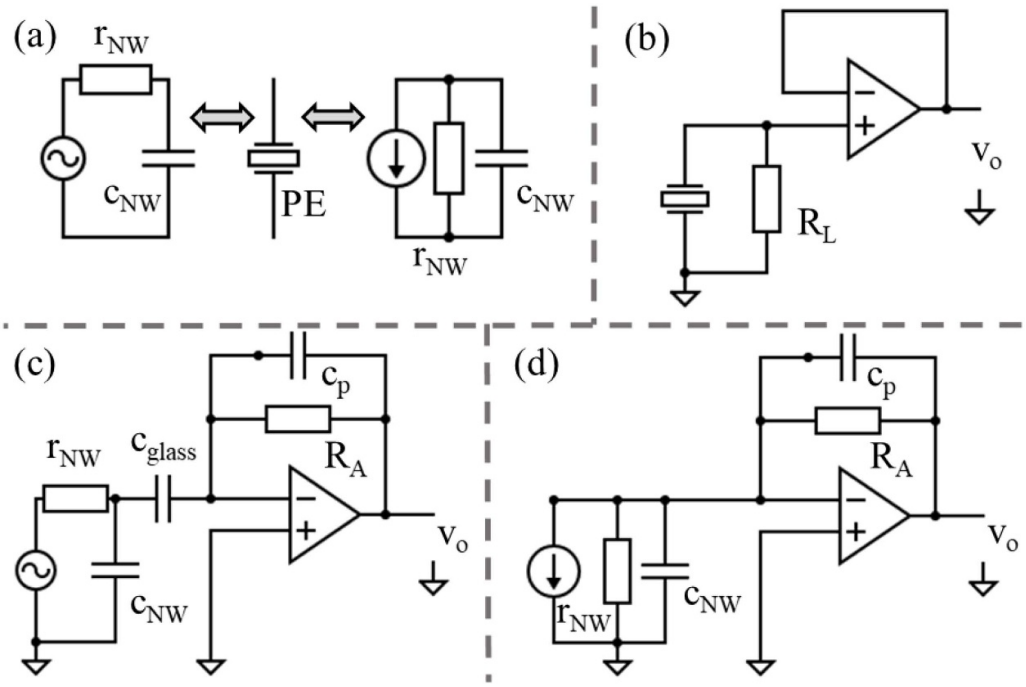

Figure 6. Electronic circuits depicting the different configurations for piezoelectric generation measurement (a) the piezoelectric element as a current or voltage source, with the NW capacitance and resistance connected in the appropriate manner; (b) the loaded resiscope mode, where neither open-circuit voltage nor short-circuit current are measured, with R_L as the load and the op-amp as a voltage follower; (c) the open-circuit configuration, realizing a voltage differentiator, with the glass slide capacitance c_{glass}, and the feedback resistor and capacitor, R_A, c_p; (d) the short-circuit configuration.

measurement), of about ± 20 nm, into account. The piezoelectric charge coefficient of GaAs is $d_{33} \simeq 1.5 - 2.5$ pm V^{-1} (pC/N) [31]. If so the application of 1300 nN should result in

$$Q = d_{33} \cdot F_{app} = 2.5 \cdot 10^{-12} \cdot 1300 \cdot 10^{-9} = 3.25 \cdot 10^{-18}\ \text{C} \tag{4}$$

Let us assume this force is reached within 0.1 sec, corresponding to the fastest ramps in figure 5. In that case, the current measured will be $Q/\Delta t = 3.25 \cdot 10^{-17}$ A. This current is in fact much lower than the noise level in our system (~ 100 fA). Moreover, even if we consider a material with $d_{33} = 100$ pC/N, and a force 100 times stronger, the current will still be roughly within the noise limit. Indeed, Gomez *et al* circumvented this limitation by using an external current amplifier in their direct-PFM application [25]. They measured relatively strong piezoelectric materials, having a flat topography. We therefore conclude that the short circuit AFM configuration, where the piezoelectric charge coefficient dominates [44], is mostly not suitable for the measurement of piezoelectric current generation. When considering that it is in fact a single NW measurement, this result is not surprising, and corresponds with previous criticism of single NW current generation [21, 22]. This also corroborates to our observation and conclusion above that other current mechanisms prevail in this configuration, and are probably what has been measured in previous work utilizing short-circuit cAFM. The piezoelectric charge (strain) coefficient, d, is directly measurable under the application of constant electric field and monitoring of strain, *i.e.* PFM mode.

3.5.2. Open-circuit configuration. We move forward to the open-circuit configuration, where the boundary conditions hold $D_{boundary} = 0$ [45, 46]. The relevant coefficient under zero displacement field is g_{33}, which is the ratio of electric field to applied stress - the piezoelectric voltage constant. As discussed above, in our configuration the voltage is not measured directly but the current in the circuit is recorded. This current is linearly related to the voltage time derivative (equation (1)).

To extract the voltage related to the application of the force we integrate the current. We focus on the charging part of the time-resolved force-current curves (ramp approach). Figure 7 shows that charge for several NWs, as a function of cantilever ramping rate, obtained by numerically integrating the current up to the point where peak-force is reached (figure 5). As discussed earlier, there still might be parasitic mechanisms contributing to the measurement. Assuming these are linear with the contact time, the 'piezoelectric' component should be mostly dependent upon the force, rather than the time. The integrated current is therefore fitted to

$$Q = a/rate + q_{PE} \tag{5}$$

where the $1/rate$ term is proportional to contact duration (a is a constant, found by fitting), and therefore q_{PE} is the time independent charge.

The results for NW #1 indicate that for the 1300 nN force, the charge accumulated on the capacitor was 2.68 pC. As mentioned earlier, $c_{glass} = 5.3$ pF. If so, the voltage drop on the capacitor is q_{PE}/c_{glass} which yields 0.505 V. Using the NW geometry mentioned above, we find the associated electric field is

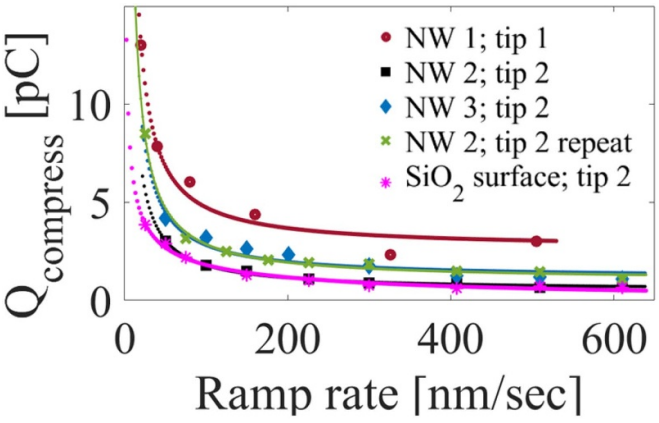

Figure 7. Integrated current during force application as a function of cantilever ramping rate (marks), and power law fitting of the data to extract the rate independent part. The results were obtained from several NWs, as well as a control experiment measured on the oxide covered surface. Doted lines are fittings according to equation 5. Tip 1 and Tip 2 are both *Adama* AD-40-AS, with force constants of 38 and 27 N/m, correspondingly.

$$E_{piezo} = V_{piezo}/L_{NW} \tag{6}$$

which yields $E_{1300nN} = 2.4$ MV/m. The associated stress is given by $T = F/A$, yielding $T_{1300nN} = 85$ MPa. Calculating the piezoelectric voltage coefficient, g_{33} (E/T), yields $g_{33,GaAs} = 0.028\,5$ Vm/N. The charge and voltage coefficients hold

$$d = g \cdot \epsilon_0 \epsilon_r \tag{7}$$

using $\varepsilon_{r,GaAs} = 13$, [47] we get a value for the charge coefficient $d_{33,GaAs} = 3.3$ pC/N. A similar analysis for two other NWs (NW 3 and the higher value for NW 2, see figure 7) yields about 1.3 pC of stored charge, and $d_{33,GaAs} = 1 - 1.2$ pC/N based on NW geometry (mostly similar to the first NW). These values are in very good agreement with known values and theoretical calculations for GaAs of 1.5-2.5 pC/N. Note that only three NW measurements are reported here, as this is a methodological paper. We plan to report comprehensive statistics in future work. A possible reason for results in the lower end of the range is that the force could contribute to bending the NW and not only compressing it, effectively reducing the apparent mechanical to electrical coupling, resulting on a lower coefficient calculated. In addition, the maximal force used here is close or over the buckling limit, indicating onset of a more complex electromechanical response; in particular, it could contribute to the lack of observed mirror peak (discharging), following possible internal discharge due internal fields in the buckled NW. Furthermore, we see the uncertainty in diameter as the main contributor to the experimental error. In the calculation, the coefficients are proportional to the diameter squared, and hence the associated error in the coefficient

is double that of the diameter, which we asses as 20% - yielding $\pm$ 40% uncertainty in the coefficients.

3.5.3. Control and further discussion. The time-resolved nature of this analysis determines the limits of the method, to be maintained for a valid analysis: 1) the ramping rate needs to be fast enough for resolving the contribution of the piezoelectric charging, and diminishing the contributions of other mechanisms (figure 7); 2) the ramping rate needs to be slow enough for the system to respond to the changes. In our case with $C \simeq$ 5 pF, and the NW resistance assessed in MΩ-GΩ, we have a time constant of $\tau = RC \simeq 10$ μS - 10 mS. This indicates that even our fastest ramps (100-200 mS long) are slow enough for the piezoelectric NW to charge the capacitor. This also indicates that the rapid peak-force operation (~ 1-2 kHz), might be too fast to measure the developed voltage, explaining the lack of measured signal in scanning mode.

We performed several control experiments to validate the measurements (Supporting Information figure S5): i) the open-circuit time-resolved procedure on the native oxide layer atop the Si growth substrate away from the NW growth area (figure 7), as well as on an unrelated sample with a top ITO electrode; ii) short-circuit time-resolved measurements of the ITO electrode; iii) short-circuit time-resolved measurements of a different GaAs NW sample, where the Si substrate is undoped. It was found that the silicon oxide layer gave rise to an electromechanical signal, which was lower, though comparable, to the integrated current during NW measurements. Although native silicon oxide is not piezoelectric, it was recently demonstrated that the AFM electromechanical apparatus is sensitive to flexoelectricity - an electrical response brought by internal strain gradient and vice-versa. Abdollahi *et al* have shown that AFM tips induce non-uniform electrical fields to layers during PFM operation, which results in the onset of the converse flexoelectric effect - manifested as an apparent piezoelectric signal [48]. Furthermore, flexoelectricity can contribute to tip-enhanced photovoltage generation [49]. It is very likely that in our case, where the direct piezoelectric effect is examined, flexoelectricity is responsible for the signals obtained from the oxide dielectric. The sharp tips used in this work (10 nm tip radius) corroborate with the quantitative analysis presented by Abdollahi and co-workers. Notably, piezoelectricity and flexoelectricity can co-exist in piezoelectric materials. When considering NWs (or rods) subjected to a vertical load by an indenter of similar dimensions, the deformation would be more uniform than that of a layer subjected to a vertical point load. This indicates that flexoelectric effects would be diminished in rods, corroborating to our analysis that the extracted quantity is indeed the piezoelectric coefficient.

Measurements on top of an ITO electrode in the open-circuit configuration (Supporting Information figure S5) gave rise to the decaying curves, similar to those measured around the current hot-spots, attributed to triboelectricity. In the short-circuit configuration, the results were entirely different: the current was 10-100 times larger, and in the opposite polarity. Finally, measurements of a similar GaAs NW grown on a non-conductive Si substrate gave a flat reading. These controls show that the current measured in the differentiator configuration is not an artefact of the system.

This method bears great implications for piezoelectric analysis at the nanoscale. As mentioned above, only a handful of reports attempt the extraction of piezoelectric coefficients from the measured data. On the one hand, using the short-circuit configuration, the generated currents are too low, and using the measurements generated by other mechanisms yield faulty results. On the other hand, the loaded configuration (resiscope mode), is neither open- nor short-circuit, making analysis more complex [19]. This leaves our open-circuit configuration as a promising alternative for the analysis of piezoelectricity in nanoscale structures, providing a applicable route to decouple various electromechanical effects.

4. Summary

The origin of our discussion is the following question: can direct piezoelectric generation of a single NW be reasonably measured in an AFM apparatus? Our answer is - yes it could. That was demonstrated using a relatively weak piezoelectric material, GaAs.

Above, we provide a comprehensive theoretical and experimental analysis for AFM-based piezoelectric generation. We demonstrated for the first time that electromechanical current mechanisms such as piezotronic, piezoelectric and triboelectric, are present in the common short-circuit configuration, and that triboelectricity and piezotronic effects dominate the measured current. These findings help settle controversy related to this type of measurement [21–23], by showing that indeed piezoelectric current generation is unlikely the effect measured, whoever other electromechanical effects are present, and could explain the results, hence they are not artifacts. We specifically show that in our configuration the triboelectric effect, and possibly photogenerated current will dominate the current sensitive scans.

We introduced an open-circuit configuration, effectively reformulating the problem from measurement of generated current, which was calculated as negligibly small for realistic piezoelectric generation, to measurement of generated voltage. We also performed time-resolved measurements of the generated current (effectively voltage differentiation). This allowed isolating and disregarding constant contributions (either real or artifacts). We demonstrated two different current mechanisms, and attributed them to triboelectric and piezoelectric generation. We extracted the piezoelectric voltage coefficient of GaAs, which is related to the piezoelectric charge coefficient, and found good agreement with values from scientific literature.

This methodology and analysis procedure will allow characterisation of nanoscale piezoelectric materials and advance the efforts of improving piezoelectric actuators, sensors and energy harvesters. As shown, it can also be used for examining triboelectric or even flexoelectric devices, depending on the dominant mechanism.

Data and Supporting Information

The data that support the findings of this study are openly available at http://doi.org/[doi]. Supporting information is available at ...

Acknowledgment

Y.C. and S.K-N. are grateful for support from ERC Starting Grant (Grant No. ERC-2014-STG-639526, NANOGEN), as well as Henry Royce Institute - Cambridge Equipment grant EP/P024947/1 and the Centre of Advanced Materials for Integrated Energy Systems ''CAM-IES'' grant EP/P007767/1. W.K., J.V.P. and A.F.i.M. thank SNF for funding through the NCCR QSIT and H2020 via project Indeed and Nanoembrace.

Appendix A. Piezoelectricity, triboelectricity and piezotronics

Research into nanoscale electromechanical phenomena has evolved from mere piezoelectricity to include a wide body of work related to the unique combination of piezoelectricity and semiconducting properties, coined as the piezotronic effect [6, 12], as well as to triboelectricity or contact electricfication [7].

Piezoelectricity. Piezoelectricity, first described by Jacques and Pierre Curie, is the linear interrelation between electrical polarisation and applied stress in non-centrosymmetric materials [50]. There are four types of piezoelectric coefficients, correlating the electric displacement D, electric field E, stress field T and strain field S [51]

$$d_{ij} = \left(\frac{\partial D_i}{\partial T_j}\right)^E = \left(\frac{\partial S_j}{\partial E_i}\right)^T \tag{A1}$$

$$e_{ij} = \left(\frac{\partial D_i}{\partial S_j}\right)^E = -\left(\frac{\partial T_j}{\partial E_i}\right)^S \tag{A2}$$

$$g_{ij} = -\left(\frac{\partial E_i}{\partial T_j}\right)^D = \left(\frac{\partial S_j}{\partial D_i}\right)^T \tag{A3}$$

$$h_{ij} = -\left(\frac{\partial E_i}{\partial S_j}\right)^D = -\left(\frac{\partial T_j}{\partial D_i}\right)^S \tag{A4}$$

indices *i,j* follow Voigt notation, *e.g.* d_{ij} describes the i component of polarisation in response to stress applied in the j direction, or alternatively strain in the j direction in response to an electric field along the i direction. The two alternative descriptions describe the direct (left-hand side equality) and converse (right-hand side) piezoelectric effect. The superscripts indicate differentiation under constant or zero fields. This has a bearing on the application of the relation to experimental conditions, depending on the boundary conditions. For example, a clamped piezoelectric structure operates under zero strain condition and will develop stress following the application of an electric signal. Alternatively, a structure clamped on one side operates under zero or constant stress. This is the operational condition of PFM, where an electric field is applied to the sample, and the strain is monitored - a direct measurement of the out of plane converse piezoelectric strain coefficient d_{jj} (alternatively named the piezoelectric charge coefficient when considering the direct effect). The application of these equations to the direct piezoelectric effect will be discussed below in detail.

The coefficients are superpositioned with the linear mechanical or electrical equations to yield the complete linear electromechanical relations, for example

$$D = \epsilon_T E + dT \tag{A5}$$

$$S = d^t E + s_E T \tag{A6}$$

where ε is the dielectric permittivity of the material, subscript T represents constant stress, d is the piezoelectric charge tensor, and d^t is the transpose of d (the interchangeably used piezoelectric strain tensor). s_E is the elastic compliance at constant electric field. Notably, the piezoelectric charge coefficient, d, is used in short-circuit configuration (constant or zero electric field), where the piezoelectric element is treated as a current source. In an open-circuit configuration the piezoelectric voltage coefficient, g, is used - where the piezoelectric element is treated as a voltage source. Piezoelectricity has many practical applications, including in sensing and actuation, however, there is a common thread to them: piezoelectricity is a decaying phenomenon. As such, only changes in stress yield useful electrical signals, and the main avenue of applications is in the AC regime.

Triboelectricity. Triboelectricity or contact electrification is a result of charge transfer between materials with different surface charge affinity [7]. Despite the literal meaning, triboelectricity can happen through mere material contact and rubbing is not a must. Triboelectricity is not limited to semiconductors or metals, or crystalline materials, and is a property of soft and biomaterials as well [52]. The interest in nanoscale triboelectricity has peaked in the past decade due to the enhanced surface area of nanomaterials, significantly increasing the efficiency of triboelectric power generation [7, 10, 52]. Similar to piezoelectricity, triboelectricity is also instantaneous. It occurs upon contact between the two materials, and decays with the reduction of the driving force for charge transfer (*e.g.* surface potential equilibrium).

Piezotronics. The research into semiconductor nanowire piezoelectricity has brought into focus the combination of semiconducting and piezoelectric properties in a single material - the piezotronic effect. [6, 11, 53] Briefly, the main characteristic of a semiconductor is the ability to tune its conductivity through application of an electric field (for example in a field effect transistor), as well as through physical contact with a different material for example, a depletion region in a pn junction or a metal-semiconductor contact). When it comes to

piezoelectricity, depletion, or lower conductivity, is associated with higher piezoelectric responses. The piezotronic effect therefore describes the effect strain has on a semiconductor device, in particular the change of an energy barrier height due to changes in the interface charge, induced by the application of stress. [54] The adequate physical treatment of this phenomena is not significantly different than that of non-ideal metal-semiconductor contacts having interface states within the band-gap, as suggested by Bardeen [55, 56]. The piezotronic effect takes the form

$$\Delta\phi_B = \phi_{B,PT} - \phi_{B,0} \sim P_{piezo} \tag{A7}$$

where the difference between the unperturbed barrier height ($\phi_{B,0}$) and the strained barrier height ($\phi_{B,PT}$) is proportional to the polarisation (P_{piezo}).

There are two important distinctions between the piezotronic effect and the piezoelectric effect, from which it originates: i) the piezotronic effect does not decay, and the barrier height change (equation (A7)) holds as long as the strain is held; ii) the piezotronic effect results in an exponential relation between the device current and the applied strain/stress, unlike piezoelectricity which is a linear effect by nature. This is due to the exponential relation between the current and the barrier height. This fact presents tremendous promise for piezotronic pressure and strain sensors, as we have recently demonstrated using GaAs NWs similar to the ones examined in this work [57].

Appendix B. Nanowire mechanics

The bending (cantilever) and compression (axial) force constants of a typical NW are given by

$$k_{bending} = \frac{3YI}{L^3} \longrightarrow \frac{Ya^4}{4\,L^3} \tag{B8}$$

$$k_{axial} = \frac{YA}{L} \longrightarrow \frac{Ya^2}{L} \tag{B9}$$

where Y is Young's modulus, I is the second moment of inertia, L the NW length, A is NW cross section area, and a is the edge of a hypothetical square cross-sectioned NW. The Euler critical load for buckling is given by (up to a constant related to the boundary fixture)

$$F_{buckling} \simeq \frac{\pi^2 YI}{L^2} \sim \frac{Ya^4}{L^2} \tag{B10}$$

For a moderate aspect ratio square cross-section NW, 1 μm long and 100 nm wide, with a Young's modulus of 100 GPa, we get $k_{axial} = 1000$ N/m, while $k_{bending} = 2.5$ N/m. The critical load for buckling is roughly 10 nN. It is therefore clear that bending standard NWs is generally much easier than compressing them. For the NWs examined here (roughly 0.2 μm long and 140 nm wide) the obtained results are $k_{axial} \simeq 10000$ N/m, while $k_{bending} \simeq 1200$ N/m; the critical buckling load is about 1000 nN. Therefore the structure is less prone to bending or instability for a given top deformation.

ORCID iDs

Yonatan Calahorra https://orcid.org/0000-0001-9530-1006
Anna Fontcuberta i Morral https://orcid.org/0000-0002-5070-2196
Sohini Kar-Narayan https://orcid.org/0000-0002-8151-1616

References

[1] Alanne K and Cao S 2019 An overview of the concept and technology of ubiquitous energy *Appl. Energy* **238** 284–302
[2] Güniat L, Caroff P and i Morral A F 2019 Vapor phase growth of semiconductor nanowires: Key developments and open questions *Chem. Rev.* **119** 8958–71
[3] Zhao M-H, Wang Z-L and Mao S X 2004 Piezoelectric characterization of individual zinc oxide nanobelt probed by piezoresponse force microscope *Nano Lett.* **4** 587–90
[4] Wang Z L and Song J 2006 Piezoelectric nanogenerators based on zinc oxide nanowire arrays *Science* **312** 242–6
[5] Wang X, Zhou J, Song J, Liu J, Ningsheng X and Wang Z L 2006 Piezoelectric field effect transistor and nanoforce sensor based on a single ZnO nanowire *Nano Lett.* **6** 2768–72
[6] Wang Z L 2010 Piezopotential gated nanowire devices: Piezotronics and piezo-phototronics *Nano Today* **5** 540–52
[7] Wang Z L 2013 Triboelectric nanogenerators as new energy technology for self-powered systems and as active mechanical and chemical sensors *ACS nano* **7** 9533–57
[8] Briscoe J and Dunn S 2015 Piezoelectric nanogenerators–a review of nanostructured piezoelectric energy harvesters *Nano Energy* **14** 15–29
[9] Zhu G, Lin Z-H, Jing Q, Bai P, Pan C, Yang Y, Zhou Y and Wang Z L 2013 Toward large-scale energy harvesting by a nanoparticle-enhanced triboelectric nanogenerator *Nano Lett.* **13** 847–53
[10] Choi Y S, Jing Q, Datta A, Boughey C and Kar-Narayan S 2017 A triboelectric generator based on self-poled Nylon-11 nanowires fabricated by gas-flow assisted template wetting *Energy Environ. Sci.* **10** 2180–9
[11] Frömling T, Roumeng Y, Mintken M, Adelung R and Rödel Jurgen 2018 Piezotronic sensors *MRS Bull.* **43** 941–5
[12] Wang C-H, Liao W-S, Nai-Jen K, Yi-Chang Li, Chen Y-C, Li-Wei T and Liu C-P 2014 Effects of free carriers on piezoelectric nanogenerators and piezotronic devices made of GaN nanowire arrays *Small* **10** 4718–25
[13] Gogneau N, Galopin E, Guilet S, Travers L, Harmand J-C and Houzé Fedéric 2014 Gan nanowires for piezoelectric generators *Phys. Status Solidi* **8** 414–19 Pascal Chrétien
[14] Gogneau N, Jamond N, Chrétien P, Houzé F, Lefeuvre E and Tchernycheva M 2016 From single iii-nitride nanowires to piezoelectric generators: New route for powering nomad electronics *Semicond. Sci. Technol.* **31** 103002
[15] Liu G, Zhao S, Henderson R D E, Leonenko Z, Abdel-Rahman E, Zetian Mi and Ban D 2016 Nanogenerators based on vertically aligned InN nanowires *Nanoscale* **8** 2097–106
[16] Mikulik D, Ricci M, Tütüncüoglu G, Matteini F, Vukajlovic J, Vulic N, Alarcon-Llado E and 2017 Anna Fontcuberta i Morral. Conductive-probe atomic force microscopy as a characterization tool for nanowire-based solar cells *Nano Energy* **41** 566–72
[17] Su W S, Chen Y F, Hsiao C L and Tu L W 2007 Generation of electricity in GaN nanorods induced by piezoelectric effect *Appl. Phys. Lett.* **90** 063110
[18] Alekseev P A, Sharov V A, Geydt P, Dunaevskiy M S, Lysak V V, Cirlin G E, Reznik R R, Khrebtov A I, Soshnikov I P

and Lähderanta E 2018 Piezoelectric current generation in wurtzite GaAs nanowires *Phys. Status Solidi* **12** 1700358
[19] Wang X, Song J, Zhang F, Chengyu H, Zheng H and Wang Z 2010 Electricity Generation based on One-Dimensional Group-III Nitride Nanomaterials *Adv. Mater.* **22** 2155–8
[20] Jegenyes N, Morassi M, Chrétien P, Travers L, Lu L, Julien F, Tchernycheva M, Houzé F and Gogneau N 2018 High Piezoelectric Conversion Properties of Axial InGaN/GaN Nanowires *Nanomaterials* **8** 367
[21] Alexe M, Senz S, Schubert M A, Hesse D and Gösele U 2008 Energy harvesting using nanowires? *Adv. Mater.* **20** 4021–6
[22] Schubert M A, Senz S, Alexe M, Hesse D and Gösele U 2008 Finite element method calculations of ZnO nanowires for nanogenerators *Appl. Phys. Lett.* **92** 122904
[23] Wang Z L 2009 Energy harvesting using piezoelectric nanowires–A correspondence on "Energy Harvesting Using Nanowires?" by Alexe et al *Adv. Mater.* **21** 1311–15
[24] Hong S, Tong S, Park W I, Hiranaga Y, Cho Y and Roelofs A 2014 Charge gradient microscopy *Proc. Natl Acad. Sci.* **111** 6566–9
[25] Gomez A, Gich M, Carretero-Genevrier A, Puig T and Obradors X 2017 Piezo-generated charge mapping revealed through direct piezoelectric force microscopy *Nat. Commun.* **8** 1113
[26] Kwon O *et al et al* 2018 Direct probing of polarization charge at nanoscale level *Adv. Mater.* **30** 1703675
[27] Calahorra Y, Smith M, Datta A, Benisty H and Kar-Narayan S 2017 Mapping piezoelectric response in nanomaterials using a dedicated non-destructive scanning probe technique *Nanoscale* **9** 19290–7
[28] Gruverman A and Kalinin S V 2006 Piezoresponse force microscopy and recent advances in nanoscale studies of ferroelectrics *J. Mater. Sci.* **41** 107–16
[29] Collins L, Liu Y, Ovchinnikova O and Proksch R 2019 Quantitative Electromechanical Atomic Force Microscopy arXiv preprint arXiv:1904.06776
[30] Minary-Jolandan M, Bernal R A, Kuljanishvili I, Parpoil V and Espinosa H D 2012 Individual gan nanowires exhibit strong piezoelectricity in 3d *Nano Lett.* **12** 970–6
[31] Calahorra Y, Guan X, Halder N N, Smith M, Cohen S, Ritter D, Penuelas J and Kar-Narayan S 2017 Exploring piezoelectric properties of III–V nanowires using piezo-response force microscopy *Semicond. Sci. Technol.* **32** 074006
[32] Hasan Md R, Baek S-H, Seong K S, Kim J H and Park I-K 2015 Hierarchical ZnO nanorods on Si micropillar arrays for performance enhancement of piezoelectric nanogenerators *ACS Appl. Mater. Interfaces* **7** 5768–74
[33] Johar M, Hassan M, Waseem A, Ha J-S, Lee J and Ryu S-W 2018 Stable and high piezoelectric output of GaN nanowire-based lead-free piezoelectric nanogenerator by suppression of internal screening *Nanomaterials* **8** 437
[34] Yang R, Qin Y, Dai L and Wang Z L 2009 Power generation with laterally packaged piezoelectric fine wires *Nat. Nanotechnol.* **4** 34
[35] Colombo C, Spirkoska D, Frimmer M, Abstreiter G and Morral A F i 2008 Ga-assisted catalyst-free growth mechanism of GaAs nanowires by molecular beam epitaxy *Phys. Rev.* B **77** 155326
[36] Matteini F, Tütüncüoglu G, Potts H, Jabeen F and Morral A F i 2015 Wetting of Ga on SiOx and Its Impact on GaAs nanowire growth *Crystal Growth Design* **15** 3105–9
[37] Matteini F, Tütüncüoglu G, Mikulik D, Vukajlovic-Plestina J, Potts H, Leran J-B, Craig Carter W and Morral A F i 2016 Impact of the Ga droplet wetting, morphology and pinholes on the orientation of GaAs nanowires *Crystal Growth Design* **16** 5781–6
[38] Pittenger B, Erina N and Su. C 2010 Quantitative mechanical property mapping at the nanoscale with peakforce qnm *Appl. Note Veeco Instrum. Inc.* 1–12
[39] Sharov V A, Alekseev P A, Borodin B R, Dunaevskiy M S, Reznik R R and Cirlin G E 2019 Inp/si heterostructure for high-current hybrid triboelectric/photovoltaic generation *ACS Applied Energy Mater.* **2** 4395–401
[40] Rocha Je G, Goncalves L M, Rocha P F, Silva M P and Lanceros-Mendez S 2009 Energy harvesting from piezoelectric materials fully integrated in footwear *IEEE Trans. Ind. Electron.* **57** 813–19
[41] Jeong C K, Park K-I, Ryu J, Hwang G-T and Lee K J 2014 Large-area and flexible lead-free nanocomposite generator using alkaline niobate particles and metal nanorod filler *Adv. Funct. Mater.* **24** 2620–9
[42] Crossley S and Kar-Narayan S 2015 Energy harvesting performance of piezoelectric ceramic and polymer nanowires *Nanotechnology* **26** 344001
[43] ECCOSTOCK dielectric materials chart
[44] Calahorra Y, Canlin O, Boughey C and Kar-Narayan S 2018 Piezoelectric semiconducting nanowires *Semiconductors and Semimetals* vol 98 (Amsterdam: Elsevier) pp 445–78
[45] Li Y L, Hu S Y, Liu Z K and Chen L Q 2002 Effect of electrical boundary conditions on ferroelectric domain structures in thin films *Appl. Phys. Lett.* **81** 427–9
[46] Eliseev E A, Kalinin S V and Morozovska A N 2015 Finite size effects in ferroelectric-semiconductor thin films under open-circuit electric boundary conditions *J. Appl. Phys.* **117** 034102
[47] GaAs basic properties Ioffe Institute
[48] Abdollahi A, Domingo N, Arias I and Catalan G 2019 Converse flexoelectricity yields large piezoresponse force microscopy signals in non-piezoelectric materials *Nat. Commun.* **10** 1266
[49] Yang M-M, Kim D J and Alexe M 2018 Flexo-photovoltaic effect *Science* **360** 904–7
[50] Curie J and Curie P 1882 Phénomènes électriques des cristaux hémièdres à faces inclinées *J. Phys. Theorique Et Appl.* **1** 245–51
[51] Damjanovic D 1998 Ferroelectric, dielectric and piezoelectric properties of ferroelectric thin films and ceramics *Rep. Prog. Phys.* **61** 1267
[52] Jing Q and Kar-Narayan S 2018 Nanostructured polymer-based piezoelectric and triboelectric materials and devices for energy harvesting applications *J. Phys. D: Appl. Phys.* **51** 303001
[53] Zhou J, Yudong G, Fei P, Mai W, Gao Y, Yang R, Bao G and Wang Z L 2008 Flexible piezotronic strain sensor *Nano Lett.* **8** 3035–40
[54] Keil P, Klein A, Rödel Jurgen and Novak N 2017 Piezotronic effect at schottky barrier of a metal-zno single crystal interface *J. Appl. Phys.* **121** 155701 Till Frömling
[55] Bardeen J 1947 Surface states and rectification at a metal semi-conductor contact *Phys. Rev.* **71** 717
[56] Sze S M and Ng K K 2006 *Physics of Semiconductor Devices* (New York: Wiley)
[57] Calahorra Y, Husmann A, Bourdelain A, Kim W, Vukajlovic-Plestina J, Boughey C, Jing Q, Morral A F i and Kar-Narayan S 2019 Highly sensitive piezotronic pressure sensors based on undoped GaAs nanowire ensembles *J. Phys. D: Appl. Phys.* **52** 294002